Key Engineering Materials
ISSN: 1662-9795, Vol. 1047, pp 1-9

Submitted: 2025-11-11
Revised: 2026-02-11
Accepted: 2026-02-14
Online: 2026-04-13

Rib Geometry in FDM of Light Alloys

Carlo Bruni[1,a*]

[1]DIISM – Università Politecnica delle Marche, via Brecce Bianche Ancona

[a*]c.bruni@univpm.it

Keywords: modeling, FDM, rib geometry.

Abstract. The present paper got the objective to propose and apply a methodology based on plastic behaviour modeling of a magnesium alloy AZ31 and on a Navier-Stokes approach to describe the rib geometry during printing by FDM (Fused deposition modeling). By the plastic modeling the rib section in terms of equivalent radius is obtained by the application of an already proposed constitutive equation under semisolid condition. The same information is obtained by the calculation of dynamic viscosity coefficient of the material under different conditions of nominal extruder nozzles that are 0.36 and 0.06 mm in radius with related extrusion velocity and internal pressure. The rib radius obtained by the plastic model is higher when the big nozzle is used compared with that given by the Navier- Stokes approach while an opposite behaviour is evidenced with the small nozzle where the apparent viscosity is higher. Increasing printing velocity similar rib dimensions are obtained in both cases.

Introduction

In the field of additive manufacturing the extrusion base techniques are very useful to realize the discretization of the material by which to produce complex shapes (double curvature surfaces, connections between curved and planar parts, multiple faceted surfaces, etc.) [1]. In fact high is the discretization, meaning low thickness values, high is the complexity of the geometry to be potentially generated. This is possible by obtaining very thin layers to be applied in any direction at working speed as high as possible comparable with that obtained during idle motion [1-4].

Such technologies known in the field of semisolid materials as FDM (Fused Deposition Modeling) can be applied successfully directly with metals when the material behaviour is known and correctly described [5-9] instead of more classic deposition modeling of bound particles and sintering [1]. The significant variable is in general represented by the temperature and by the pressure inside the extruder allowing the material flow [5-11]. Both of such variables can be tuned in order to represent a positive effect on the material deposition on the platform. Other variables are in general the geometry of the extruder and printing machine parameters [9-11].

Some authors report applications on titanium, magnesium and aluminium alloys in order to realize prismatic objects starting by the material knowledge under semisolid conditions [2-4,6,7,11]. They observed a overall decrease in internal stress with increasing temperature due to semisolid condition achieved. Similar results were obtained by the author in previous works on magnesium alloys [7,12] once approaching high strain rates leading to a faster achievement of semisolid condition due to heat generated. Even if the initial stress levels could appear naturally higher than those described.

This behaviour promotes high production rates also in prototyping phase in order to shorten the design stage by high printing velocities together with the discretization useful to manage very thin layers and complex surfaces. These objectives to be achieved at the same time in the field of light metal alloys need a modeling phase with which to describe the material also under the conditions of high pressure inside the extruder with micro-dimension diameters [9,11,13].

Many authors [8,9,11,14,15] approach the solution of the problem to describe FDM to get very thin layers by different methods based on analytics, on finite element simulation by different explicit/implicit algorithms, on discrete element methods, mesh less, discrete events, etc. Up today the analytical modeling represents the fastest and save costing way to approach the problem even if under defined hypotheses.

The framework of the reported field can be updated with the following proposed methodology based on analytical modeling in which two different approaches are considered. The one based on extrusion plastic modeling in which the constitutive equation of a AZ31 [12] magnesium alloy is adopted in order to describe high strain rate semisolid ribs obtained with deformation and friction heating contributions evaluated in previous works under similar or less heavy conditions [7] starting by a temperature of 400°C. The other one based on Navier-Stokes fluid dynamic equation proposed in a form to get the dynamic viscosity coefficient under semisolid by which to calculate the rib thickness. The obtained results at under millimeter rib dimension are similar to each other when printing velocities increase.

Modeling Procedures

The methodology reported in Fig.1 consists in two modeling approaches based on flow behaviour knowledge of material updated to consider semisolid condition in one case and in a fluid dynamics approach based on Navier-Stokes equation to calculate the dynamic viscosity coefficient. The material bahaviour is described in order to get the thickness of the layer function of different variables.

Modeling by plastic behaviour of material is applied by an analytical model of extrusion considering the slab method when the semiconical angle approaches 90°. In the described condition material flow promotes 45° angle under high temperatures at solid state. That is the conical part of extruding tool as reported in previous works by the author [7] where friction, deformation and distortion heating produce a rapid increase in temperature by the 400°C initially tuned. The conditions are similar to those reported in the cited work, in which a initial radius of 0.6 is deformed to the nominal 0.3, completed with a study concentrated on the initial radius of 0.36 mm deformed to 0.06. The solid/liquid fraction is considered under similar hypotheses. The rib section dimensions obtained by the modeling of the plastic behaviour and the one by the fluid dynamics approach are compared to each other.

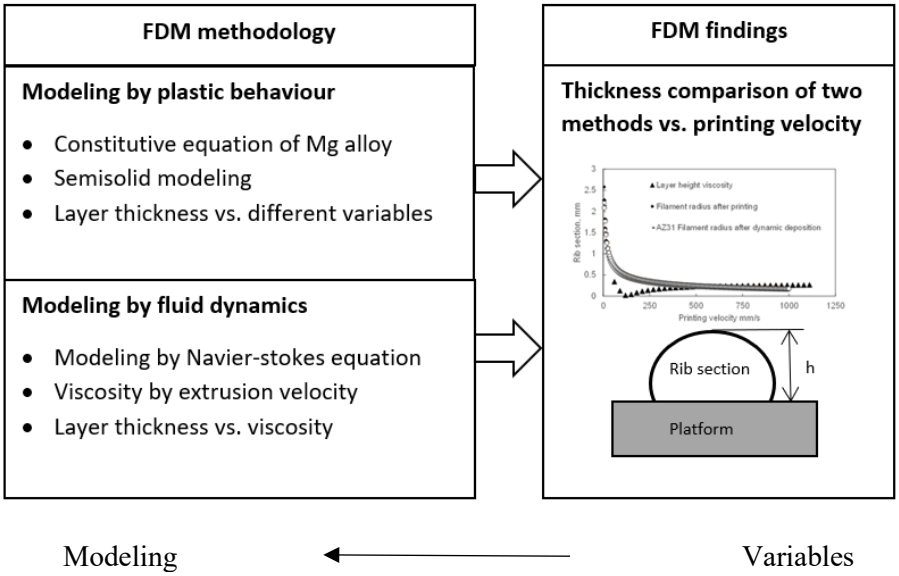

Fig. 1. Modeling procedure.

When applying the first model the stress amount is calculated with the following equation:

$$\sigma_z = \frac{2\cdot\bar{\sigma}\cdot\ln\left(\frac{R_0}{R_f}\right)R_0^2}{R_f(2\cdot R_0 - R_f)}\cdot\exp\left(\frac{2\mu}{R_0}\Delta l_{def}\right) \quad (1)$$

where:
σ_z: tension at the stem of the container
σ: material flow
μ: friction coefficient

R_0: initial billet radius
R_f :final billet radius
Δl: travel covered by the stem
The total stress amount can be calculated considering the fraction of the solid by respect to one of completely solid. In the formulation the factors of 0.2 and 0.3 for friction and distortion phenomena are implemented [7].
The tension amount in the extrusion chamber is given by:

$$\sigma_{extr} = \frac{2\cdot\bar{\sigma}\cdot\ln\left(\frac{R_0}{R_f}\right)R_0^2}{R_f(2\cdot R_0 - R_f)} \quad (2)$$

The flow behaviour of material is reported by the power law based approach [7,12]:

$$\bar{\sigma} = K\cdot\bar{\varepsilon}^n\cdot\dot{\varepsilon}^m \quad (3)$$

In which K, n, m are material constants being $\varepsilon = 2\cdot\ln(R_0/R_f)$ and $\dot{\varepsilon} = \varepsilon/\Delta t$ while 0.1 represents the part to be multiplied in order to model the semisolid state.
Once calculated the absolute stress amount the pressure interval evaluation inside the extruder is reported by the following:

$$\Delta\sigma_{\text{extrusion solid fraction}} \approx \Delta p \quad (4)$$

The already reported formulas allow to determine the equilibrium equation given as follows:

$$\rho\cdot V\cdot g\cdot\Delta h + \rho\cdot V\cdot\frac{\Delta v_y}{\Delta t}\Delta h = \sigma\cdot\Delta\varepsilon\cdot V \quad (5)$$

Being the v_y the velocity along the direction perpendicular to the platform and Δh the shortening of material in form of layer once arrived to the surface of that. The previous equation can be developed in:

$$\rho\cdot g\cdot\Delta h + \rho\cdot\frac{\Delta v_y}{\Delta t}\Delta h = K\cdot\left(\frac{\Delta v_y}{h_0}\right)^m\cdot\left(\frac{\Delta h}{h_0}\right)^n\cdot\frac{\Delta h}{h_0} \quad (6)$$

Considering the density that can be represented as a function of temperature [16,17]

$$\rho = \rho_0 - 0.23\cdot(T - 30) \quad (7)$$

displacement of the upper surface of the layer at contact with the platform is evaluated in terms of:

$$\Delta h = \sqrt[n]{\frac{\rho\cdot\left(\frac{\Delta v}{\Delta t}+g\right)}{k\cdot\left(\frac{\Delta v}{h_0}\right)^m\cdot\left(\frac{1}{h_0}\right)^{n+1}}} \quad (8)$$

The results obtained by the proposed analytical modeling are plotted in terms of the difference $h=h_0-\Delta h$. They are compared with those obtained by the analytical modeling of the second approach.
In particular, it is based on Navier-Stokes model described by the following applied equation:

$$\rho\frac{\Delta v}{\Delta t} + \rho v\frac{\Delta v}{\Delta y} = -\frac{\Delta p}{\Delta y} + k\left(\frac{\Delta v}{\Delta x}\right)^2 \quad (9)$$

It can be used in the form of the following:

$$\mu = k' = \frac{\rho\Delta v\left(\frac{1}{\Delta t}+v\frac{1}{\Delta y}\right)+\frac{\Delta p}{\Delta y}}{\left(\frac{\Delta v}{\Delta x}\right)^2}\frac{\Delta z}{\Delta t} \quad (10)$$

to calculate the dynamic viscosity coefficient μ.
In the same equation:
v= velocity along the y axis (parallel to the extruder nozzle)
Δv= velocity variation along the y axis
Δx, Δy, Δz = the dimensions of the volume considered
Δp= pressure variation inside/outside the extruder
By the above equation the shear stress normally reported in terms of $\tau = \mu\cdot\dot{\gamma} = \mu\cdot\Delta l/(\Delta y\cdot\Delta t)$ gives:

$$\Delta l = \frac{\Delta y \cdot \Delta t \cdot \tau}{\mu} \quad (11)$$

$$\Delta l' = \frac{\Delta l}{\sqrt{3}} \quad (12)$$

The values obtained by the described equations allow to evaluate the thickness of the layer by the constant volume hypothesis and then the $h=h_0-\Delta h$ where h_0 is described for both the models by the following:

$$h_0 = D_{rib} = \sqrt{\frac{0.8 \cdot v_{extr} \cdot D_{extr}^2 \cdot t}{L}} \quad (13)$$

By that value the equivalent radius of the layer thickness is evaluated as $r=(h_0 - \Delta h)/2$ depending also on extruding velocity, nozzle diameter and printing velocity L/t.
The reduction in thickness due to shrinkage can be calculated considering the decrease in temperature until ambient by the following:

$$r_f = \alpha \cdot r \cdot \Delta T \quad (14)$$

With α dilatation coefficient and ΔT temperature variation.

Results

The pressure inside the container in terms of stress can be estimated mainly with eqs. 1 to 3 through the material behaviour knowledge at the solid reported in [7]. It is adapted in order to consider the strain rates typical of the extruding ratios above described approximating hundreds of 1/s with coefficient 0.1 to describe semisolid. Fig. 2 reports the stress trend characterized by an increase at the exit as in more conventional extrusion operations. The obtained values to reach the filament radius of 0.06 mm are higher than those already reported in previous works where the strain rates and extruding ratios were lower.

Obviously when used for load sizing the eq. 1 must be applied at the end of displacement in which the stress values are calculated with eq. 2 at the maximum. Even if such evaluation is not the objective of the investigation being the value at the stem obtained by the value at the beginning of the extrusion chamber.

Instead, the values obtained in the forming chamber can be considered for Δp evaluation with eq. 4 inside the extruder on a length not higher than 0.3 mm. Following the values in terms of stress, Δp can be approximated to about 800 MPa being low the stress amount given by the constitutive equation at semisolid.

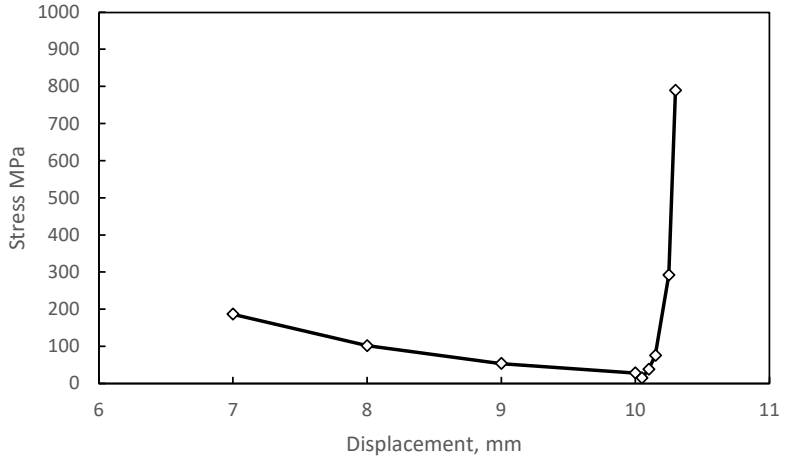

Fig. 2. Stress behaviour inside the extrusion container for AZ31 magnesium alloy at nominal nozzle radius of 0.06 mm.

Considering the equilibrium energy of eq. 5 in order to get information by eqs. 6 to 7 the Δh when material drops to the platform surface can be calculated by eq. 8.

The other method based on viscosity evaluation at extruding velocity of 360 mm/s through an extruding radius of 0.06 mm allows the obtaining $3.60 \cdot 10^4$ Pa·s. To the purpose eqs. 9 and 10 are used with density of material of eq. 7.

By those the h amount is calculated by the knowledge of Δl being the material deformation under semisolid along the axis parallel to the platform evaluated by eq. 11 and eq. 12 as reported in the modeling procedure.

The results are reported initially in Fig. 3 in terms of section equivalent radius obtained by an half of the actual layer thickness h versus printing speed including the constat flow rate described by the eq. 13. It can be observed a decrease in equivalent radius mainly with printing speed. The effect of cooling in terms of geometry variation can be extremely negligible so that it can be overcome in subsequent threats.

In Fig. 4 the calculation of dynamic apparent viscosity using eq. 10 versus pressure is reported considering the working interval by 800 MPa revealed inside the extruder up to 1000 MPa when a quasi-hydrostatic condition needs to be realized without changes in any other variable. The results substantially agree with that found in [6].

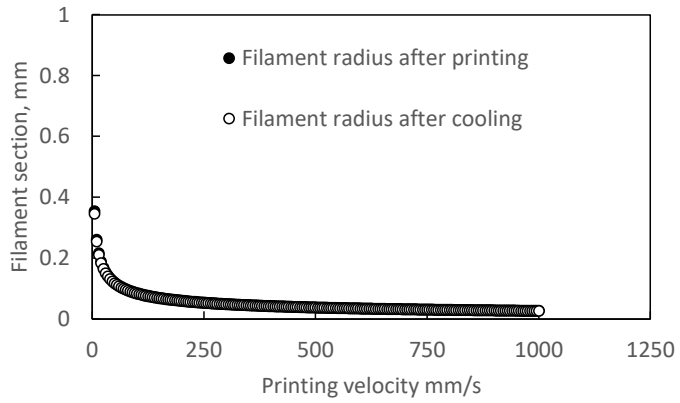

Fig. 3. Rib equivalent radius with semiplastic modeling function of printing velocity for nominal nozzle value of 0.06 mm.

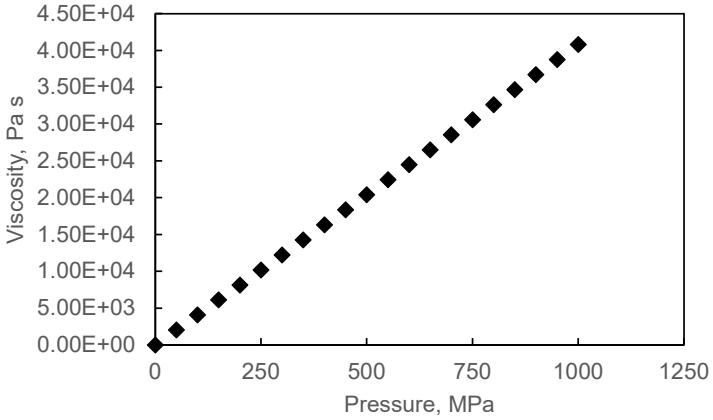

Fig. 4. Viscosity values at different pressures.

Fig. 5 reports the rib equivalent radius vs. printing velocity with values of viscosity obtained by eq. 10 with layer thickness h calculated by the constant volume hypothesis. It is plotted vs. printing velocity considering the material flow dependent on the velocity outside the extruder.

The comparison between the rib behaviour obtained by the plastic model and that given by the Navier-Stoke equation based one is reported in Fig. 6 for nozzle radius of 0.06 mm. The high values

of viscosity obtained as reported in Fig. 3 determine low values of Δh. In Fig. 7 the values are reported in the case of higher nominal nozzle radius 0.36 mm. The lower values of the rib equivalent radius vs. printing velocity curve obtained by the fluid dynamic model with respect to those of plastic model are due to different apparent viscosities obtained.

Similar behaviours in both extruding ratios are obtained by two models at high printing speed representing the significant variable of the metal FDM under investigation. This means the possibility to obtain high curvatures typical of those required for complex geometries as in conventional polymer additive manufacturing.

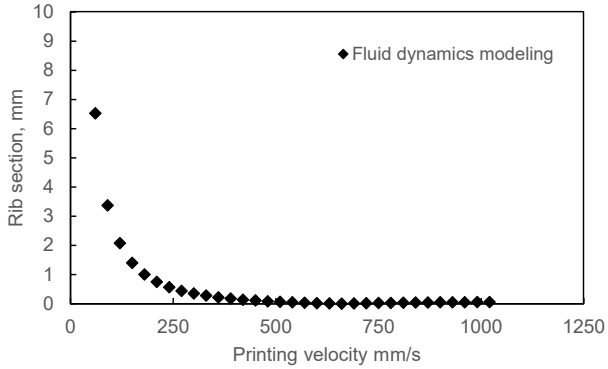

Fig. 5. Equivalent radius obtained with fluid dynamic modeling function of printing velocity for nominal nozzle radius of 0.06 mm.

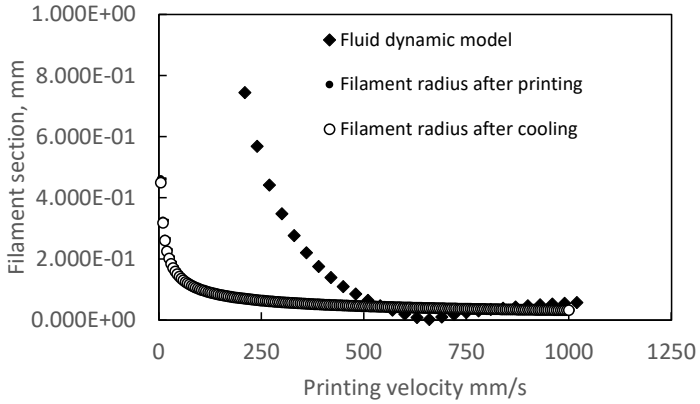

Fig. 6. Comparison between plastic and fluid dynamic models in describing rib equivalent radius with extruder nozzle at 0.06 mm.

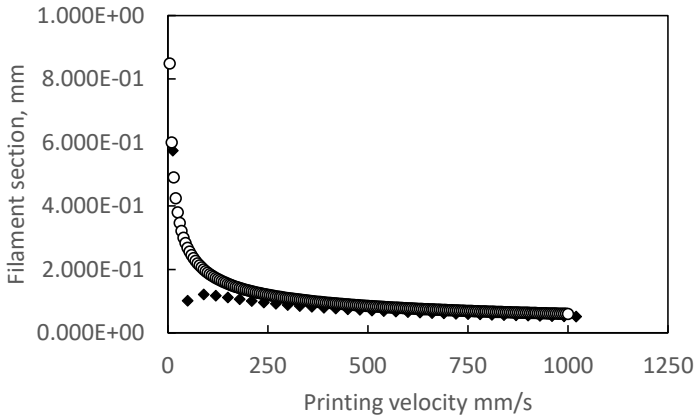

Fig. 7. Comparison between plastic and fluid dynamic models in describing rib equivalent radius with extruder nozzle at 0.36 mm.

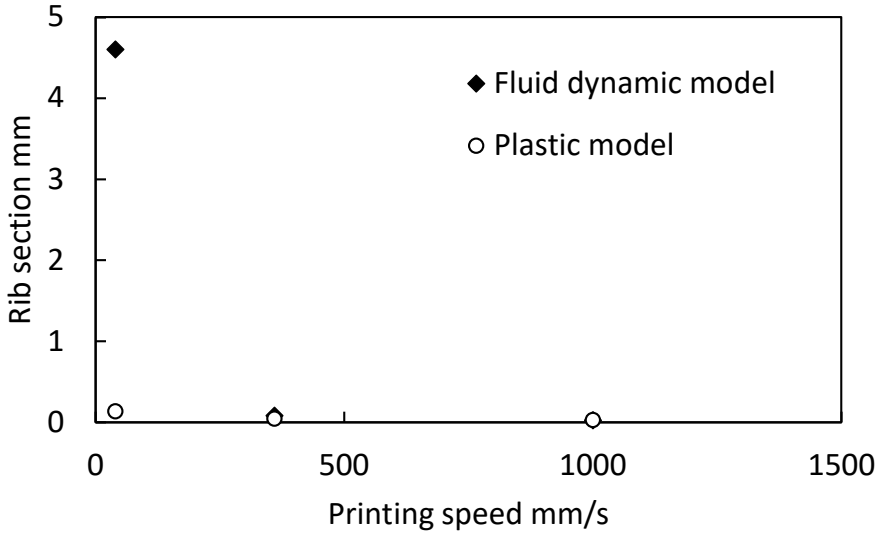

Fig. 8. Comparison between layer radii obtained by semisolid plastic model and fluid dynamic model at extruder diameter of 0.06 mm.

Being the effect of temperature decrease negligible as reported previously due to the requirement to keep temperatures of the extruding system not higher than 600-630°C in order to maintain the solid fraction of 0.1 according to the melting map [13], rib dimension is mainly dependent on the other variables according to that found in [6,10,18] under similar conditions.

To the purpose Fig. 8 reports synthetically the results of the rib layer in terms of the main variable represented by printing velocity when the extruding nozzle of 0.06 mm in radius is considered. Values by 0.134 mm at 40 mm/s to 0.026 mm at 1000 mm/s in the case of plastic model are obtained being 0.024 mm that given by the fluid dynamic model at the highest speed studied. The difference is about 0.84 % in last case. At 0.36 mm nozzle radius it can be observed that for given printing velocities of 40, 360 and 1000 mm/s the rib section in terms of equivalent radius tends to be similar for two modeling approaches in particular at high printing speeds. Some considerations could be done also at $\Delta p = 0$ with similar results.

Summary

Computing the layer thickness through the rib radius vs. nozzle dimension, extrusion velocity and printing velocity is the object of the investigation. Two approaches are proposed and followed. The one based on plastic modeling of the material considering semisolid at temperatures not higher than 600-630°C in order to maintain the semisolid fraction of 0.1. The other one starting by the Navier Stokes equation through viscosity evaluation in order to determine the elongation of the rib and subsequent layer thickness in terms of equivalent radius.

It is observed that layer thickness evaluated with plastic behaviour model descreases with increasing printing speed representing the main variable of the modeled FDM system where the effect of cooling appears negligible and that of the nozzle radius arises when the printing speed approaches the extrusion velocity. In particular, higher values are obtained by the fluid dynamic model compared with ones of plastic model for the extrusion nozzle of 0.06 mm. While lower values are given for the highest value of the nozzle. Such behaviour can be due to the increased value of relative apparent viscosity obtained being higher the pressure inside the extruder when the nominal 0.06 mm in radius is considered for analysis. The rib section described by both the models in terms of equivalent radius is similar when the printing speed is increased.

References

[1] B. Liu, Y. Wang , Z. Lin, T. Zhang, Creating metal parts by Fused Deposition Modeling and Sintering, Materials letter 263 (2020) 127252. https://doi.org/10.1016/j.matlet.2019.127252.

[2] T. Schuller, M. Jalaal, P. Fanzio, F. J. Galindo-Rosales, Optimal shape design of printing nozzles for extrusion-based additive Manufacturing, Additive Manufacturing 84 (2024) 104130. https://doi.org/10.1016/j.addma.2024.104130.

[3] H. Yu, W. Zhang, B. Yin, W. Sun, A. Akbar, Y. Zhang, K.M. Liew, Modeling extrusion process and layer deformation in 3D concrete printing via smoothed particle hydrodynamics, Computer Methods in Applied Mechanics and Engineering 420 (2024) 116761. https://doi.org/10.1016/j.cma.2024.116761.

[4] J. A. Naranjo, C. Berges, A. Gallego, G. Herranz, A novel printable high-speed steel filament: Towards the solution for wear-resistant customized tools by AM alternative, Journal of Materials Research and Technology, 11 (2021) 1534-1547. https://doi.org/10.1016/j.jmrt.2021.02.001.

[5] S. Altıparmak, Victoria A. Yardley, Z. Shi, J. Lin. Extrusion-based additive manufacturing technologies: State of the art and future perspectives, Journal of Manufacturing Processes, 607–636. (2022). https://doi.org/10.1016/j.jmapro.2022.09.032.

[6] G. C. Nzebuka, C. O. Ufodike, A. M. Rahmane, M. B. Minus, C. P. Egole, Thermal-fluid modeling and simulation of Ti-6Al-4V alloy filaments during shaping in the hot-end of material extrusion additive manufacturing, Journal of Manufacturing Processes 131 (2024) 866–878. https://doi.org/10.1016/j.jmapro.2024.09.040.

[7] C. Bruni, Semisolid deposition of metallic material by extrusion-base analytical and simulative methodologies, Materials Research Proceedings 44 (2024) 433-44. https://doi.org/10.21741/9781644903254.

[8] C. Bruni, M. El Mehtedi, F. Gabrielli, Flow curve modelling of a ZM21 magnesium alloy and finite element simulation in hot deformation, Key Engineering Materials Vols. 622-623 (2014). https://doi.org/10.4028/www.scientific.net/KEM.622-623.588.

[9] Qi. Wang, L. Wang, J. Xu, H. Zhai, Y. Chen, S. Xia, X. Qin, Y. Li, B. Jiang, D. Chen, Extrusion limit diagram of Mg–5Bi–3Al–1Zn alloy and effects of extrusion parameters on its microstructures and mechanical properties. Journal of Materials Research and Technology 29 (2024) 5166–5179. https://doi.org/10.1016/j.jmrt.2024.02.182.

[10] Z. Zhang , S. Xia , X. Chen , L. Wang, Q. Wang , J. Xu , X. Qin , M. Ali , W. Wang , W. Huang, B. Jiang. Achieving ultra-high extrusion speed and strength-ductility synergy in a BAZ531 magnesium alloy via differential-thermal extrusion Materials Science and Engineering: A, 923 2025 147687. https://doi.org/10.1016/j.msea.2024.147687.

[11] Xi. Huo, B .Zhang, Q. Han, Y. Huang, J. Yin, Numerical simulation and printability analysis of fused deposition modeling with dual-temperature control, Bio-Design and Manufacturing (2023) 6:174–188. 7. https://doi.org/10.1007/s42242-023-00239-1.

[12] C. Bruni et al., Constitutive models for AZ31 Magnesium alloys, Key Engineering Materials, 36. https://doi.org/10.4028/www.scientific.net/KEM.367.87.

[13] J. Feng, D. Zhang, H. Hu, Y. Zhao, X. Chen, B. Jiang, F. Pan, Improved microstructures of AZ31 magnesium alloy by semi-solid extrusion, Materials Science & Engineering A 800 (2021) 140204. https://doi.org/10.1016/j.msea.2020.140204.

[14] N. Bontcheva , G. Petzov , L. Parashkevova, Thermomechanical modelling of hot extrusion of Al-alloys,followed by cooling on the press, Computational Materials Science 38 (2006) 83–89. https://doi.org/10.1016/j.commatsci.2006.01.009.

[15] Y. Dewang, J. Raghuwanshi,V. Sharma, Finite element analysis of extrusion process using aluminum alloy, Materials Today: Proceedings 24 (2020) 500–509. https://doi.org/10.1016/j.matpr.2020.04.302.

[16] R. N. Abdullaev, R. A. Khairulin, Yu. M. Kozlovskii, A. Sh. Agazhanov, S. V. Stamkus. Density of magnesium and magnesium–lithium alloys in solid and liquid states, Nonferrous Met. Soc. China 29(2019) 507−514. doi: 10.1016/S1003-6326(19)64959-9.

[17] T. A. Osswald, J. Puentes, J. Kattinger. Fused filament fabrication melting model, Additive Manufacturing 22 (2018) 51–59. https://doi.org/10.1016/j.addma.2018.04.030.

[18] Y. G. Mittal, G. Gote, Y. Patil, A. K. Mehta, P. Kamble, K.P. Karunakaran, Investigations on ironing parameters in screw extrusion additive manufacturing, Manufacturing Letters 41 (2024) 822-831. https://doi.org/10.1016/j.mfglet.2024.09.102.